Contrib Mineral Petrol (1982) 80:262–275

Contributions to Mineralogy and Petrology

The Colima Volcanic Complex, Mexico: III

Ash- and Scoria-Fall Deposits from the Upper Slopes of Volcán Colima

James F. Luhr and Ian S.E. Carmichael
Department of Geology and Geophysics, University of California, Berkeley, California 94720, USA

Abstract. A 34 meter section of ash- and scoria-fall units has been studied on the upper NE flank of the active Volcán Colima. Charcoal and soil horizons are restricted to the topmost 12 m. Nine ^{14}C dates show a smooth progression from 235 years near the surface to 8,300 years at 10 meters depth, indicating a post-Pleistocene accumulation rate of 1.3 m/1,000 years at 6 km from the vent. This figure allows an estimate of the magmatic eruption rate for fall-material of 0.31 km^3/1,000 years, less than 15% of Colima's lava eruption rate. An unusually thick and coarse-grained scoria-fall horizon at about 4 m depth in the section appears to have been produced by the caldera-forming eruption of Colima some 4,300 years ago.

The majority (40) of 46 analyzed scoria and ash horizons are typical Colima hornblende-andesites with an average SiO_2 content of 58%, nearly identical to the scoriae of Colima's 1913 pyroclastic flows. The scoriae are significantly more basic than Colima's andesitic lavas, which average 61% SiO_2. The six remaining scoria horizons are anomalously alkalic and rich in incompatible elements. Five coarse alkaline scoria layers occur in sequence just below the 8,300 year level. They show progressive upward increases in K, P, Ba, Sr, Zr, La, Ce, and related elements, culminating in a phlogopite-bearing scoria horizon.

Over the last 20,000 years or so, a group of cinder cones erupted 20–35 km to the north of Volcán Colima, producing basic alkalic magmas including basanites and phlogopite-bearing minettes. The alkaline scoriae of the studied sections probably record pre-eruptive injections of minette magma into the subvolcanic, calc-alkaline system of V. Colima. The age, composition, and mineralogy of the alkaline scoriae are consistent with this interpretation. Least squares mixing models suggest 60 wt.% minette component in the phlogopite-bearing horizon.

Introduction

Volcán Colima is a large, active andesitic volcano at the western end of the Mexican Volcanic Belt. Its geologic setting is discussed in Luhr and Carmichael (1980, 1981; subsequently referred to as LC-I and LC-II). In brief, V. Colima marks the southern end of a southward younging chain of three composite volcanoes which formed on the floor of the N-S trending Colima graben during the Quaternary. In this area, the N-S convergence of the N. American and Cocos Plates is overprinted by the E-W extension of the Colima graben system. Volcanism in the area is also anomalous; in addition to the large composite volcanoes dominated by calc-alkaline andesite, nine cinder cones formed on the lower flanks of these volcanoes in the late-Quaternary, erupting a variety of basic alkalic magmas ranging from basanites to minettes.

Volcán Colima is the most active volcano in Mexico, having experienced numerous pyroclastic and lava eruptions during the 400 years of observational record (LC-I, Luhr 1981). The dominant eruptive product of Colima is hornblende-andesite. As a result of its frequent pyroclastic eruptions, the volcano is covered by a thick mantle of hornblende-bearing pyroclastic deposits. The abundance of hornblende and pyroclastic deposits at V. Colima underscore the relatively hydrous nature of its magmatic system.

An earlier study (LC-I) primarily considered historic and prehistoric lavas of V. Colima's post-caldera cone, but also included scoriae from the pyroclastic-flow eruption of 1913. The focus of this paper is on the pyroclastic-fall portion of V. Colima's eruptive budget, as represented by a thick layered sequence of ash- and scoria-fall deposits exposed in roadcuts on the NE (downwind) flank of the volcano. The stratigraphy and ^{14}C dating of this sequence are discussed in the next section, followed by a treatment of compositional and mineralogical data from 46 scoria and ash horizons.

Field Relations

The active cone of V. Colima is centered in the southern half of a prominent caldera 5 km in diameter (Fig. 1). The flanks of its ancestral volcano and the much larger Pleistocene volcano Nevado, to its north, are covered by a thick blanket of pyroclastic deposits. The walls of long-lived stream canyons often show pyroclastic-flow units interbedded with fluvial sands and conglomerates, while the higher ground is covered by a mantle of bedded ash- and scoria-fall layers, tens of meters in total thickness. Charcoal-bearing soil horizons are common in the fall-deposits, and charcoal is widespread in Colima's pyroclastic-flow deposits.

Waitz (1906) was the first to speculate on the origin of Colima's caldera, describing it as a maar for unknown reasons. Demant (1979) recognized the extent of pyroclastic deposits draping the Colima volcanoes as well as the increasing degree of alteration with depth in most ash- and

Reprint requests to: J.F. Luhr

0010-7999/82/0080/0262/$02.80

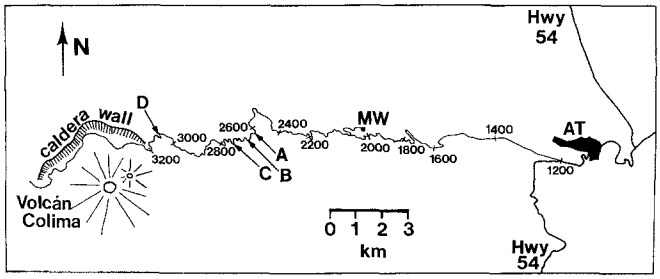

Fig. 1. Map showing the logging road running from Hwy 54 into the caldera of V. Colima. Elevations in meters along the road are indicated. The locations of the four pyroclastic sections A–D are also shown. *AT*: Atenquique; *MW*: microwave tower

Table 1. Location data for pyroclastic sections A–D

	d (km)	elev (m)	d_{VC} (km)
Hwy 54	0	1,200	18.0
A	20.9	2,640	6.1
B	21.8	2,700	5.6
C	22.8	2,760	5.2
D	27.6	3,120	2.6
Caldera entrance	29.5	3,200	2.2

d = distance along logging road from Hwy 54
elev = approximate elevation for the midpoint of each section
d_{VC} = map view distance from the crater of V. Colima

scoria-fall sections, and suggested that Colima's caldera resulted from cyclical ash and scoria eruptions. Pyroclastic eruptions have continued into the present century at V. Colima (Luhr 1981), but high erosion rates within the caldera and near the caldera rim quickly remove unconsolidated ash and scoria. As a result, stratigraphic-structural relationships between the caldera scarp and ash- and scoria-fall units are not observed.

Colima's caldera wall is highest (340 m) to the north, adjacent to the older volcano Nevado. The elevation of the caldera rim drops steadily to the SW and SE, where it is eventually buried by lavas of the post-caldera cone. The active cone grew in the southern portion of the caldera, continuing the progressive southward migration of volcanism in the Colima-Cantaro chain (LC-II). The lower southern slopes of Colima are covered by 5–300+ m thick chaotic volcanic breccias consisting of large, dense lava blocks encased in a fine-grained matrix. Juvenile fragments are rare to non-existent. The deposits cover at least 300 km^2 in a 90° sector extending 20 km southward from the present crater, and display prominent hummocky topography. These chaotic deposits are similar to dry-avalanche deposits (Aramaki 1979; Ui 1981) or rockslide-avalanche deposits such as those generated during the May 18, 1980 collapse of the north face of Mt. St. Helens (Voight et al. 1981). Aramaki (1979) defined dry-avalanche deposits as formed by large-scale sector collapse of a volcanic cone. V. Colima's southward-opening, horseshoe-shaped caldera appears to have formed in such a manner. Charcoal collected from just below the avalanche unit has been dated at 4,300 years (unpublished data), which we believe represents the age of Colima's caldera. As discussed below, the caldera-forming avalanche was associated with an estimated 0.35 km^3 of pyroclastic-fall material and an unknown volume of pyroclastic flows.

The studied ash- and scoria-fall sequence is exposed in cuts along a logging road which joins Hwy 54 just SW of Atenquique, and runs 29.5 km due west up the NE flank of V. Colima, reaching the entrance to the caldera after gaining 2,000 m (Fig. 1). Four isolated sections along this road were investigated. The locations of these four sections (A–D) are shown in Fig. 1; Table 1 gives location data for the sections, relative to the road junction with Hwy 54. Stratigraphic columns are shown in Fig. 2, where prominent

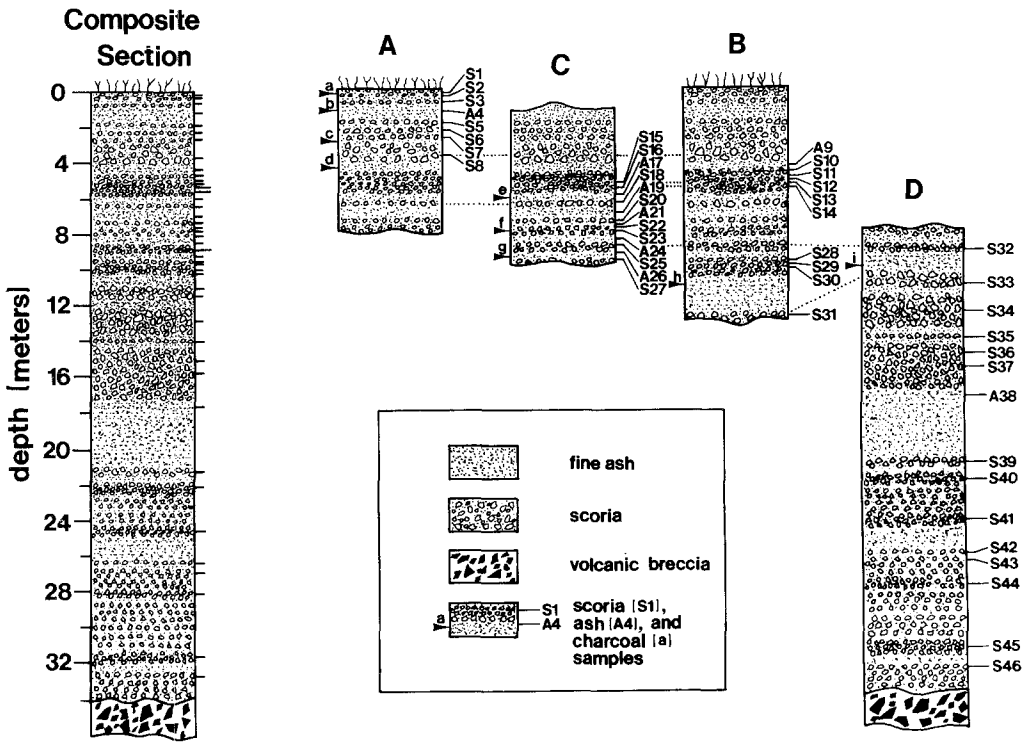

Fig. 2. Generalized stratigraphic columns for the pyroclastic sections A–D and a composite section. Individual section locations are marked on Fig. 1 and described in Table 1. Sampled scoria and ash horizons are described in Appendix 1

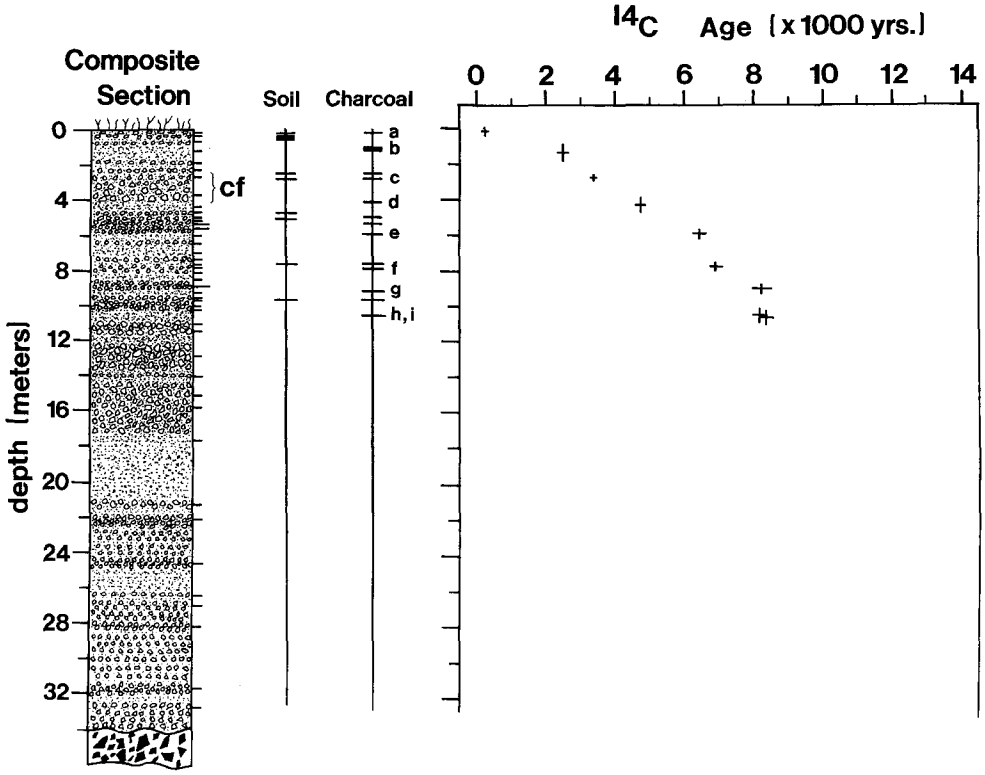

Fig. 3. Locations of soil horizons and sampled charcoal, and a plot of nine ^{14}C ages listed in Table 2 versus stratigraphic depth. "cf" indicates scoria layer S8 from the caldera-forming eruption

ash and scoria horizons are distinguished. These four isolated sections were combined into a composite section 34 m in total thickness; correlations between sections were based on prominent key beds or sequences of beds, ^{14}C ages from interbedded charcoal samples, and modal and compositional analyses of scoria and ash samples. The composite section is shown on the left of Fig. 2.

^{14}C Ages

Figure 3 shows the locations of prominent soil horizons in the composite section. Charcoal is common within these soil horizons and also occurs as carbonized twigs in beds of fine ash. Thirteen sampled charcoal horizons are also indicated on Fig. 3. Nine of these charcoal samples were dated by ^{14}C analysis at Teledyne Isotopes. The ages and uncertainties are listed in Table 2 and plotted on Fig. 3 as error crosses. The width of each cross corresponds to the uncertainties reported in Table 2, and the height corresponds to the thickness of the charcoal-bearing bed. Figure 3 shows a smooth increase in ages from 235 yrs below the surface scoria to >8,200 yrs at 10 m depth. The three oldest ages (g, h, i) from between 10 and 12 m depth are indistinguishable. Volcán Colima has experienced numerous historical pyroclastic eruptions, with three Pelean-type events punctuating eruptive cycles in 1611, 1818, and 1913 (LC-I and Luhr 1981). Each appears to have produced an elongate ash-fall zone oriented toward the northeast, the direction of the studied sections. The mantle of ash- and scoria-fall deposits covering the volcano has probably accumulated from these great eruptions, separated by a century or more. Within the uncertainty of the underlying ^{14}C date, the uppermost scoria S1 may correspond to the 1818 eruption. The ash- and scoria-fall deposit from the 1913 eruption has not been identified in the studied sections. As mentioned above, Colima's caldera formed from sector collapse of the cone about 4,300 years ago (Fig. 3 – cf). The carbon ages listed in Table 2 leave no doubt that the caldera-forming eruption produced the thick (140 cm), normally-graded, and coarse-grained (up to 10 cm) scoria-fall layer S8 (Fig. 2 and App. 1), whose base is at 4 m depth in the composite section. This layer is underlain by charcoal sample 'd' (4,740 years) and overlain by charcoal sample 'c'

Table 2. ^{14}C age determinations on charcoal samples

Charcoal sample	Section	TI#	Age (years)
a	A	I-11,968	235+/− 75
b	A	I-12,064	2,540+/−110
c	A	I-11,967	3,400+/− 95
d	A	I-12,063	4,740+/−150
e	C	I-11,606	6,450+/−180
f	C	I-11,605	6,910+/−190
g	C	I-12,062	8,230+/−270
h	B	I-11,965	8,210+/−150
i	D	I-11,966	8,360+/−150

Sample locations (see Appendix 1 for detailed stratigraphy)

a) Charcoal from 10 cm soil-ash underlying scoria S1
b) Charcoal from upper part of 1 m ash bed A4
c) Charcoal from 20 cm soil-ash underlying scoria S7
d) Charcoal from upper levels of ash underlying scoria S8
e) Charcoal from upper levels of ash A17
f) Charcoal from 4 cm soil-ash underlying scoria S22
g) Charcoal from ash A26
h) Charcoal from reworked ash overlying scoria S31
i) Charcoal from reworked ash between S32 and S33; equivalent to charcoal h

TI# – Teledyne Isotopes sample number

(3,400 years). It is one of the thickest and coarsest-grained horizons in the studied sections. Layers S1 to S7 erupted from Colima's post-caldera cone, while the layers below S7 were erupted from the ancestral volcano.

The age data indicate an average deposition rate of approximately 1.3 m/1,000 years, at a position 6 km from the present crater of Colima. The lack of an inflection in Fig. 3 at an age of 4,300 years indicates that formation of Colima's caldera had no impact on overall eruption rate, which has remained relatively constant for at least the last 8,000 years. By analogy with carefully studied, similarly elongate ash- and pumice-fall deposits from the 5/18/80, 5/25/80, 6/12/80, and 7/22/80 eruptions of Mt. St. Helens (Sarna-Wojcicki et al. 1981; Waitt and Dzurisin 1981; Waitt et al. 1981), it is possible to estimate a volume eruptive rate for Colima's pyroclastic-fall material. Estimated thicknesses at 6 km downwind from the vent were plotted versus estimated magmatic volumes for the four St. Helens fall units using a modification of the technique of Sarna-Wojcicki et al. (1981). A regression of these data for magmatic eruptive volumes less than 0.2 km^3 yields:

$$V_m = 0.0024\,(T_6) \qquad (R = 0.99)$$

where V_m = magmatic volume in km^3 (at 2.6 g/cm^3), and T_6 = maximum thickness in cm at 6 km from the vent. Coupled with Colima's post-Pleistocene accumulation rate at 6 km distance (1.3 m/1,000 years), this relationship indicates 0.31 km^3/1,000 years of magma erupted as ash- and scoria-fall deposits. This estimate is crude and can be improved by further studies of Colima's pyroclastic deposits. It does not include pyroclastic-flow material. The eruptive rate for fall-material is less than 15% of the estimated lava eruptive rate of 2.4 km^3/1,000 years (LC-I; Luhr 1981). The 140 cm thickness of S8 indicates that Colima's caldera-forming eruption produced some 0.35 km^3 of magma as ash- and scoria-falls.

Most ash- and scoria-fall sections at Colima show an increase in alteration with depth (Demant 1979). The ^{14}C ages obtained in this study confirm that at least the upper fall sequence was built from repeated pyroclastic eruptions over thousands of years. Boundaries between adjacent ash and scoria layers which are marked by soil horizons (Fig. 3) obviously indicate a significant hiatus between eruptions. Where soil horizons are absent, no reliable criterion could be established to indicate the length of time represented by the layer boundaries.

The absence of soil horizons and charcoal in the lower portion of the composite section is intriguing. This absence probably reflects significantly different climatic conditions in the area during the late-Pleistocene to early Holocene, which were not as conducive to soil formation. The pine forests which cover the volcano today, and which made charcoal so abundant in the younger levels, were probably not present before 8,000 years ago.

Whole Rock Chemical Compositions

Sample Preparation and XRF Major Element Analyses

The investigated ash- and scoria-fall sections show a relatively simple stratigraphic sequence. Thirty-eight scoria beds and 8 ash layers were sampled for analysis. Appendix 1 gives descriptions of the sampled horizons.

Scoria layers range in thickness from 6-190 cm; individual scoriae are generally less than 5 cm, but approach 15 cm in thick, coarse grained horizons (e.g. S8, S33, S34). Dense lithic fragments accompany vesiculated scoriae in all layers. These are generally hornblende- and pyroxene-andesites and probably represent disrupted crater dome material. Large scoriae were collected from each sampled horizon. After oven drying, they were cleaned by nylon brush and compressed air, and crushed to pea size using a tungsten carbide mortar. Slight alteration is present in most samples, particularly in those from the lower levels of the composite section. Scoria S31, which was analyzed for correlation purposes only, is badly altered. After coarse crushing, the least altered large fragments were selected and ground for 15 min in a SPEX shatterbox of tungsten carbide. Contamination by W, Co, and Ta results. For samples containing scoriae >5 cm in diameter, thin sections were cut from scoria chips. For finer scoria samples, pea-sized fragments from coarse crushing were impregnated in epoxy and sectioned.

Uninterrupted sequences of fine ash layers can reach 3 m in total thickness. Bulk ash samples were collected from eight horizons. After oven drying, they were passed through a 0.5 mm sieve to remove occasional larger scoria and lithic fragments. A split from the <0.5 mm portion was then ground for 15 min in the SPEX shatterbox, and another split was impregnated in epoxy and thin sectioned. The ashes contain $<5\%$ lithics (Appendix 3).

The 46 powders were pressed into aluminum cups at 20,000 p.s.i. These undiluted pressed powder pellets were analyzed on a United Scientific energy dispersive X-ray fluorescence machine for 10 major and 13 trace elements. The method of major element analysis is dependent upon well analyzed, compositionally similar standards. For this purpose, wet-chemically-analyzed samples discussed in LC-I and -II were used. The analyzed spectrum of each sample was separated into the 10 major elements of interest by a least squares fit. The standards were used to calibrate linear equations of counts vs. concentration for each element, which were then applied to the unknowns. Major element scoria and ash analyses generally total between 96% and 99% due to hydration. All analyses have been normalized to 100% anhydrous. One standard deviation errors calculated from the analysis of other wet-chemically-analyzed andesites and basalts treated as unknowns correspond to the following absolute amounts: SiO_2 (0.6%), TiO_2 (0.05%), Al_2O_3 (0.6%), FeO[t] (0.15%), MnO (0.02%), MgO (0.20%), CaO (0.10%), Na_2O (0.40%), K_2O (0.10%), P_2O_5 (0.03%).

Two of the most compositionally interesting scoria samples, S33 and S34, were also analyzed by wet chemistry and instrumental neutron activation. Results are given in Table 3, along with XRF trace element analyses and uncertainties.

Compositional Variations

The scoria samples are presumed to represent magmatic compositions, but the eight analyzed bulk ash samples have been subjected to air-fall sorting and to sieving, and contain up to 5% lithic fragments. Despite such complications, most ash samples plot among scoria analyses on compositional variation diagrams, demonstrating that these near-vent ashes deviate only slightly from magmatic compositions.

Table 3. Wet chemical, INA, and XRF analyses of S33 and S34

	S33	S34		S33*		S34*	
Wet chemistry			INA				
SiO_2	51.52	53.47	Na%	2.68	(0.05)	2.99	(0.06)
TiO_2	1.01	0.96	Al%	7.2	(0.2)	8.1	(0.2)
Al_2O_3	14.37	15.72	Sc	24.04	(0.07)	24.63	(0.07)
Fe_2O_3	4.56	3.51	Ti%	0.43	(0.04)	0.50	(0.04)
FeO	2.72	3.64	Cr	330	(3)	189	(2)
MnO	0.12	0.13	Mn	979	(20)	1,087	(22)
MgO	7.52	5.89	Fe%	5.39	(0.07)	5.51	(0.07)
CaO	8.18	7.94	Co	31.2	(0.4)	29.5	(0.4)
Na_2O	3.28	3.75	Ni	93	(9)	40	(9)
K_2O	2.77	2.38	Cs	0.6	(0.2)	0.4	(0.2)
P_2O_5	0.62	0.48	Ba	1,767	(30)	792	(19)
H_2O^+	1.92	1.02	La	54	(3)	34	(2)
H_2O^-	0.79	0.47	Ce	121	(1)	82	(1)
			Nd	67	(3)	49	(2)
Total	99.38	99.36	Sm	9.59	(0.04)	8.34	(0.04)
			Eu	2.54	(0.02)	2.30	(0.02)
CIPW Norm (mol%)			Tb	0.69	(0.03)	0.68	(0.03)
			Dy	3.7	(0.1)	4.0	(0.1)
qz	0.00	0.67	Yb	1.52	(0.03)	1.70	(0.03)
or	16.76	14.25	Lu	0.19	(0.02)	0.20	(0.02)
ab	30.16	34.13	Hf	6.32	(0.09)	5.12	(0.08)
an	16.70	19.29	Ta	0.237	(0.004)	0.211	(0.004)
di	16.57	13.97	Th	4.69	(0.06)	4.05	(0.06)
hy	10.02	11.59	U	1.51	(0.06)	1.34	(0.06)
ol	2.22	0.00	XRF (ppm)				
mt	4.60	3.72					
ilm	1.44	1.36					
hm	0.19	0.00	V	190		193	
ap	1.33	1.02	Cu	90		62	
			Zn	71		72	
			Ga	23		22	
			Rb	24		26	
			Sr	2,689		1,434	
			Y	21		22	
			Zr	232		198	

Wet chemical analyses by I.S.E. Carmichael
Alkalies by J. Hampel, flame photometer
INA analyses by F. Asaro and H. Michel, Lawrence Berkeley Laboratory (Perlman and Asaro 1969)
INA data in ppm except for Na, Al, Ti, and Fe. Numbers in parentheses are one standard deviation counting uncertainties
* Samples ground in agate to avoid Co-Ta contamination
XRF counting uncertainties of one standard deviation correspond to the following percentages of the amounts present: V (8%), Cr (10%), Ni (15%), Cu (12%), Zn (10%), Ga (10%), Rb (10%), Sr (5%), Y (15%), Zr (5%), Ba (3%), La (15%), and Ce (10%)

The 46 analyzed samples fall into two broad groups. The bulk of them (40 samples) are similar to post-caldera andesites of V. Colima discussed in LC-I. The other group consists of five scoriae (S20, S31, S33, S34, S35) and one ash (A38) that are relatively alkalic and enriched in incompatible elements. The arbitrary criterion for inclusion in this group is $P_2O_5 > 0.25$ wt.%.

Figure 4A shows plots of P_2O_5, K_2O, Ba, and Sr vs. SiO_2 content. Colima's post-caldera andesitic lavas (triangles; LC-I) and the basaltic scoria (open star) from a small cinder cone to its NE (LC-II) define linear trends on these four plots, and the majority of the ash (open squares) and scoria (circles) samples from the studied sections also conform to these trends. A notable aspect of this major group of pyroclastic samples is their lower SiO_2 contents compared with typical lava compositions (Fig. 4). The 33 scoria samples from this group have an average SiO_2 content of 58.0% ($1\sigma = 1.7\%$). Scoria S8 from the caldera-forming eruption contains 58.2% SiO_2 and is a typical representative of this group. In contrast, the average SiO_2 content of 24 pre- and post-caldera lavas from V. Colima and Nevado is 61.2% ($1\sigma = 1.9\%$). The lavas average 3.2% higher in SiO_2 and consequently have somewhat higher contents of incompatible elements and lower contents of compatible elements. A similar observation was made in LC-I regarding historical eruptions of V. Colima. Historical lava compositions (1869, 1961, 1975) range from 60.5–61% SiO_2, whereas scoriae from the Pelean-type eruption of 1913 contain only 57.5% SiO_2. It appears to be a general pattern for lava eruptions at V. Colima to involve significantly more silicic magmas than pyroclastic eruptions. Baker and Holland (1973) noted the same relationship between lavas and more basic pyroclastic deposits on St. Kitts in the Lesser Antilles.

The five alkalic scoria samples are plotted separately on Fig. 4 as open diamonds. They have relatively low SiO_2 contents and fall above incompatible-element trend lines for other Colima samples, lying in the compositional space between the calc-alkaline Colima suite on the one side, and the basanite-minette suite on the other (closed diamonds). As seen on Fig. 4A, the basanite-minette samples are highly enriched in incompatible elements. In the following sections we develop the idea that the five alkalic scoria samples from the studied sections represent physical, pre-eruptive mixtures of these two distinct magma series, the basalt-andesite suite of V. Colima and the basanite-minette suite. The trends on Fig. 4 are consistent with this view. The low-SiO_2, alkaline ash A38 has the mineralogy (olivine + chromite + augite) and composition of a crystal-enriched basanite ash. Its origin is discussed further below.

Figure 4B shows plots of MgO, Cr, Ni, and V vs. SiO_2 content. On average, MgO, Cr, and Ni show continuous depletion in the calc-alkaline suite from the calc-alkaline basalt (star) through the andesites (triangles, circles). The V contents of the most basic calc-alkaline basaltic andesites (54–56% SiO_2) are somewhat higher than the basalt, suggesting that V contents inititally increase with differentiation, reach a maximum near 55% SiO_2, and thereafter progressively decrease toward more SiO_2-rich compositions. Unfortunately, though, no calc-alkaline samples are available in the critical SiO_2 content range 50–54%. The V-SiO_2 relations in Fig. 4B are consistent with control by spinel fractionation. A spinel phase crystallizes throughout the calc-alkaline suite: V-poor Cr-Al-Mg-Fe spinels as inclusions in olivines of the basalt (LC-II) and basaltic-andesites, and V-rich titanomagnetites of the basaltic andesites and andesites (LC-I).

The basanite-minette compostions are again plotted on Fig. 4B as closed diamonds. Compatible element contents in this basic alkalic suite range upward from the values in the calc-alkaline basalt. The five alkaline scoriae from the studied sections are again shown as open diamonds. They generally plot near the trend lines for the calc-alkaline suite, but are not inconsistent with derivation by mixing between the calc-alkaline and basic alkaline suites.

Compositional Variations with Stratigraphic Depth

Figure 5 shows plots of P_2O_5, K_2O, and Sr versus stratigraphic depth in the composite section. The elements Ba,

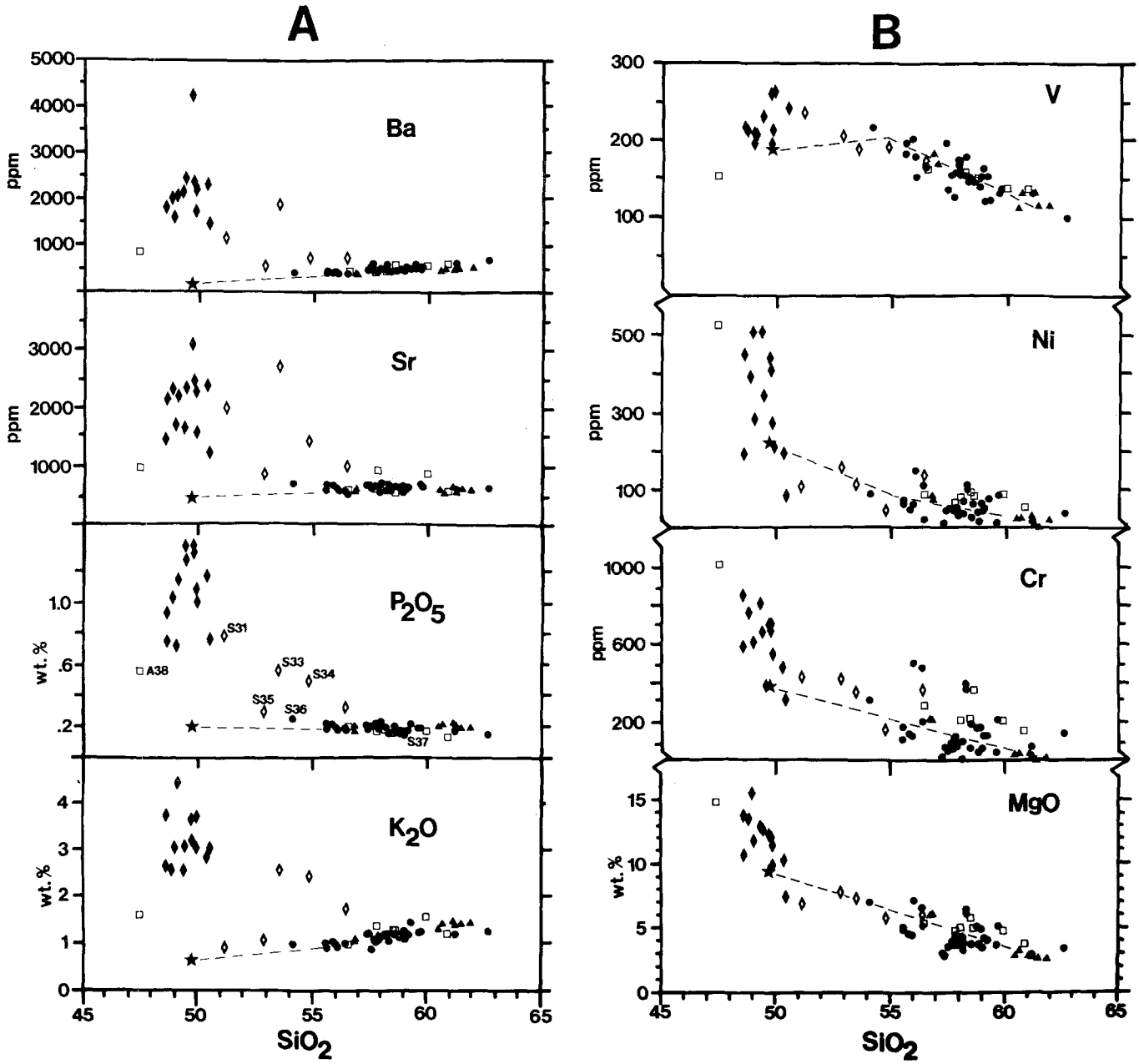

Fig. 4. A: Whole rock Ba, Sr, P_2O_5, and K_2O concentrations plotted versus SiO_2 for southern Colima graben volcanics. All data normalized to 100% anhydrous. *Triangles*: post-caldera lavas from V. Colima (LC-I). *Closed diamonds*: basanite-minette samples (LC-II). *Star*: calc-alkaline basalt (LC-II). *Circles*: calc-alkaline scoriae (this study). *Open diamonds*: alkaline scoriae (S20, S31, S33, S34, S35). *Open squares*: bulk ash samples. *Dotted lines* drawn by eye through calc-alkaline trends. *B*: Whole rock V, Ni, Cr, and MgO concentrations versus SiO_2. Symbols as in Fig. 4A. Unpublished XRF analyses of V are used for post-caldera lavas, basanites, minettes, and the calc-alkaline basalt in place of less precise INA data (LC-I and -II)

Zr, La, and Ce show similar patterns. The two major groups of pyroclastic samples are again distinguished, using the same symbols as in Fig. 4. The majority of the samples, the calc-alkaline scoria and ash, show only slight variations in P_2O_5, K_2O, and Sr with depth; K_2O and Sr contents are related to SiO_2 content as shown in Fig. 4A. There is no obvious change in eruptive composition at the level of caldera formation (cf).

The six alkalic samples have much higher contents of these and other incompatible elements. The lowest of the group, ash A38, is from a 3 m thick sequence of compositionally similar ashes in the middle of section D. As mentioned above, it has the mineralogy of a crystal-enriched basanite. A38 is interpreted as an ash erupted from one of the basanite-minette cinder cones, which lie 20–35 km to the NE and NW, and some 1,500 m lower in elevation. Considering the >8,300 year age of this ash, and the morphologically estimated ages of the basanite-minette cinder cones (LC-II), the most likely source for A38 is either V. La Erita or V. Cuauhtemoc. The 3 m thickness of A38 is baffling, however, for such vent distances. Overlying ash A38 is a 7 m sequence of ash and scoria layers with no charcoal or soil horizons. In ascending order, A38 is followed by scoriae S37 and S36, which might arguably be

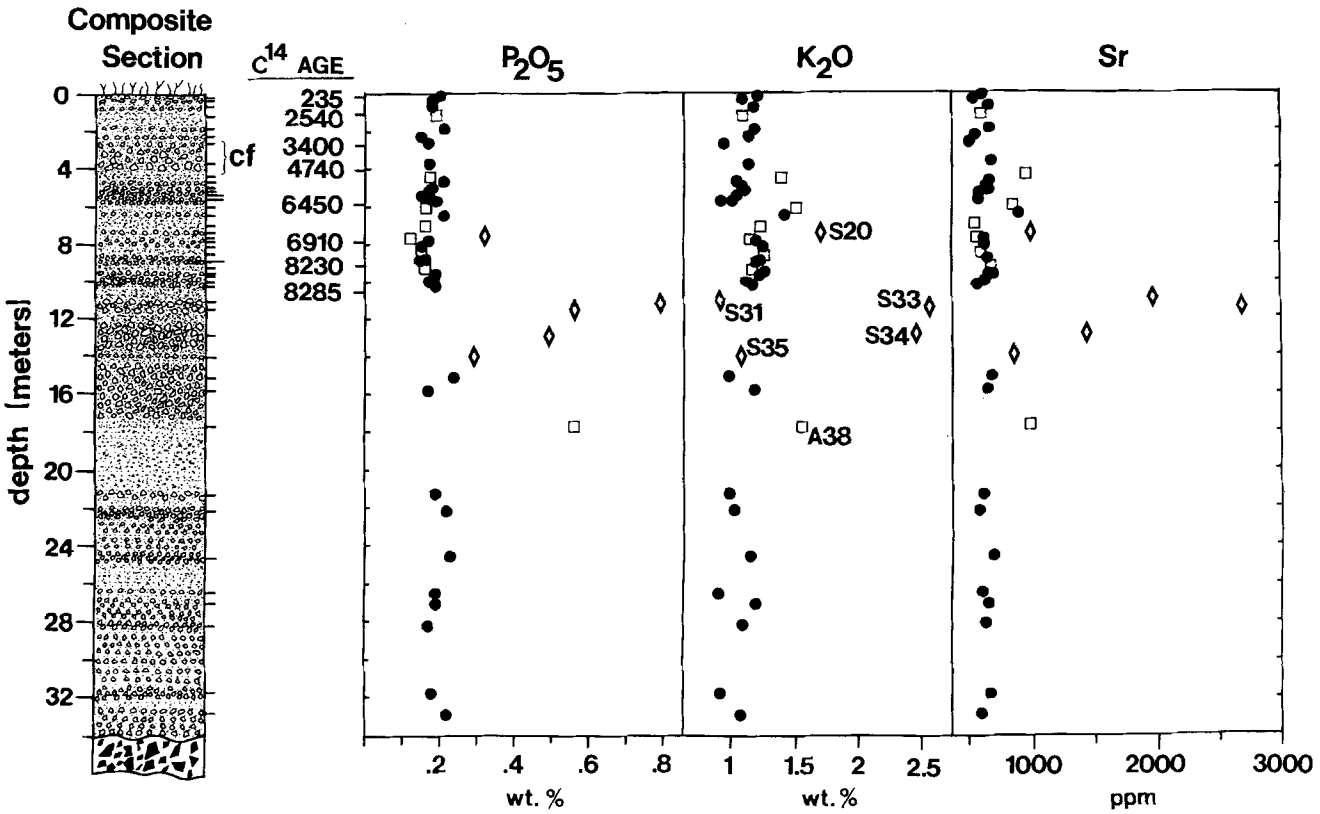

Fig. 5. Whole-rock concentrations of typical incompatible element concentrations P_2O_5, K_2O, and Sr versus stratigraphic depth. Symbols as in Fig. 4. Sample numbers are listed for the 6 alkaline scoriae and ash on the K_2O plot. Scoria S31 is badly altered and anomalously low in K_2O and Rb. "cf" as in Fig. 3

included in the alkaline group, as they show slight incompatible-element enrichments. By the classification system adopted in this paper (alkaline: >0.25% P_2O_5), S36 is the most basic calc-alkaline sample in the studied section. Overlying S36 are 3 of the 4 alkaline scoria horizons (S35, S34, S33, S31). In this ascending sequence, the concentrations of P_2O_5, Sr, Zr, and La progressively increase. S34 is the thickest (190 cm) and coarsest-grained (up to 15 cm) scoria-fall layer in the sections. S33 and S31 were both taken from the upper horizon, which contains phlogopite and represents the most extreme of the alkaline scoriae; unfortunately both are visibly altered, S31 rather badly. As a consequence, S31 shows anomalously low contents of K_2O, Rb, and Ba, and high Al_2O_3. S31 is followed upward by a 4 m thick sequence of calc-alkaline ash- and scoria-fall layers from 8,300 to 6,900 years old. These in turn are overlain by the final alkaline horizon, S20, at about the 6,800 year level. The upper 7 m of the section, covering the last 6,800 years, contains only calc-alkaline layers, including S8 from the caldera-forming eruption.

To summarize the compositional variations with time, the majority of the section consists of calc-alkaline scoriae and ashes having broadly similar contents of incompatible elements. The portion immediately underlying the oldest 14C date (8,300 years) includes an unusual series of alkaline layers. This sequence begins with a crystal-rich basanite ash, probably derived from a basanite cinder cone to the NW. It is followed by two calc-alkaline scoria horizons with slightly high incompatible element contents. One of these, S36, is the most basic of the calc-alkaline scoria group. These are followed by 3 alkaline scoria horizons just below the 8,300 year ^{14}C age, which show upward increases in incompatible elements. The highest and most alkaline of these scoria layers contains phlogopite. It is overlain by calc-alkaline ash and scoria to the surface, with the exception of the youngest alkaline scoria S20 at about 6,800 years.

Mineralogy

Mineral Abundances

Modes were determined by point counting for the 46 scoria and ash samples (Appendix 3). Phenocrysts (>0.3 mm) and microphenocrysts (>0.03 mm) were counted separately following the conventions of Wilcox (1954), and the data can be directly compared with modes determined for V. Colima's post-caldera suite (LC-I) and the basanite-minette suite (LC-II). Figure 6 shows selected plots of mineral abundances versus SiO_2 content with the different suites designated by different symbols as in Fig. 4.

To review the mineralogy of the basanite-minette series: all samples contain phenocrystic olivine (1–16 vol%) with included chromites, and later augite, which dominates as microphenocryst and groundmass crystals (Fig. 6). The basanites have rare phenocrystic plagioclase, while the minettes contain phenocrystic phlogopite (<2.5 vol%).

V. Colima's post-caldera lavas are strongly porphyritic (20–39 vol% phenocrysts; Fig. 6). Plagioclase dominates and is accompanied by bronzite, augite, and titanomagnetite in all samples. Six samples, including the lavas of 1869, 1961, and 1975, have SiO_2 contents in the range

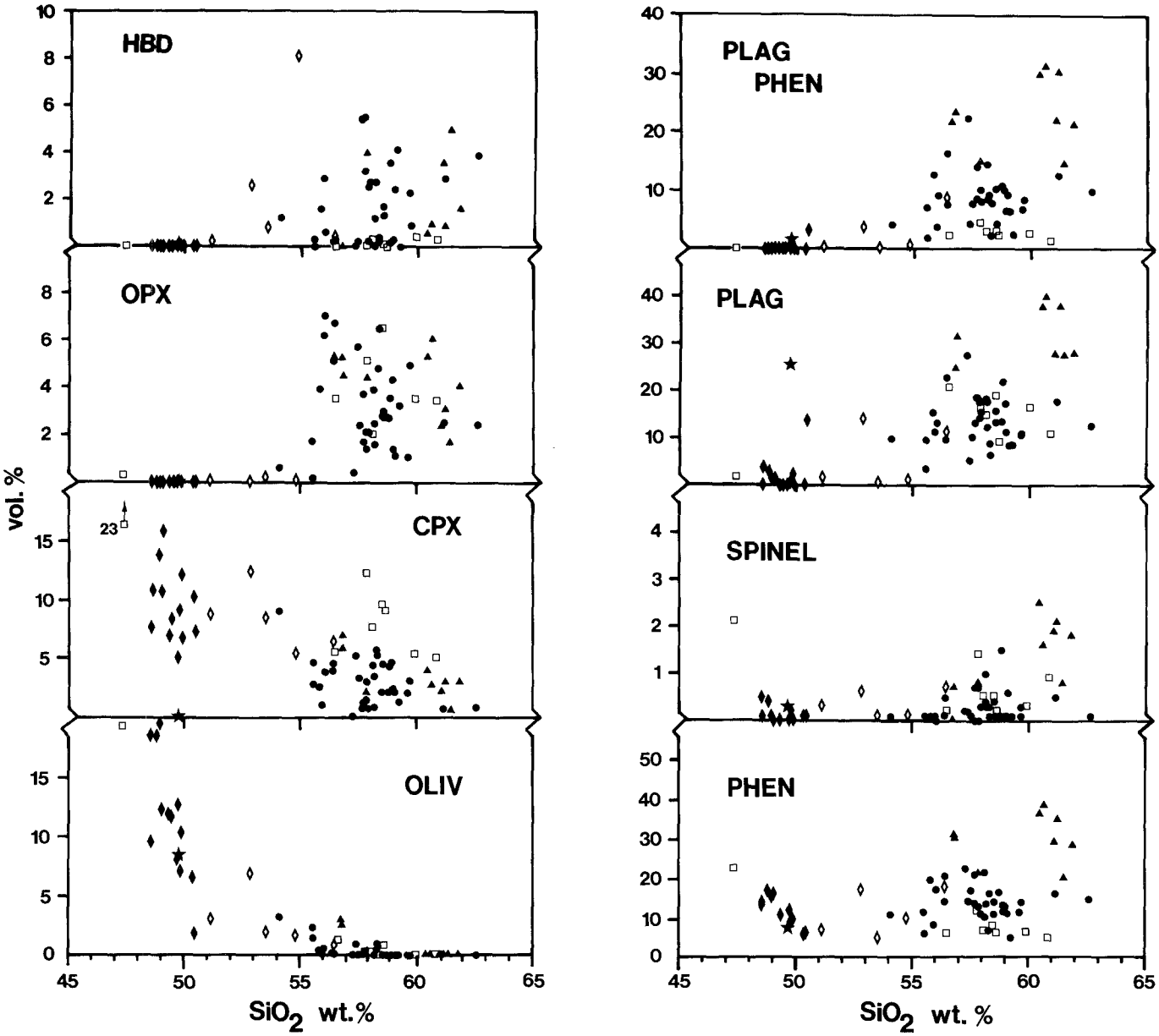

Fig. 6. Plots of modal data in vol% (taken from Appendix 3, LC-I and -II) versus whole rock SiO_2 content. Symbols as in Fig. 4. *HBD*: all hornblende; *OPX*: all orthopyroxene; *CPX*: all augite; *OLIV*: all olivine; *PLAG PHEN*: plagioclase phenocrysts (>0.3 mm); *PLAG*: all plagioclase; *SPINEL*: spinel + titanomagnetite; *PHEN*: all phenocrysts (>0.3 mm)

60.5–61.5 wt.%, contain 0.5–5 vol% hornblende, and only rare olivine relicts. Two more basic andesites (SiO_2 = 56.5%) contain 2.5–3 vol% olivine in the absence of hornblende. Scoriae from Colima's 1913 Pelean-type eruption contain 57.5% SiO_2 and differ mineralogically from the more silicic hornblende-andesite lavas only in their much lower plagioclase contents and, therefore, lower total crystal contents. The calc-alkaline basalt (LC-II) contains phenocrystic olivine with included spinel, microphenocrystic plagioclase, and groundmass augite.

The calc-alkaline scoria and ash samples from the studied sections are dominantly hornblende-bearing andesites and basaltic-andesites, with a few pyroxene-andesites, all containing plagioclase and augite (Fig. 6). Olivine occurs in many samples with <58.5% SiO_2, while bronzite contents decrease abruptly below 56% SiO_2. Most calc-alkaline scoriae are compositionally and mineralogically similar to the 1913 scoriae (LC-I) in showing relatively low plagioclase and total crystal contents compared to post-caldera lavas. The percentage of microphenocrystic spinel shows a general increase with SiO_2 content toward 2.5 vol% (as titanomagnetite) in the hornblende-andesite lavas. When compared with calc-alkaline scoriae, the bulk ashes show broadly similar mineral abundances; they have probably undergone little fractionation from magmatic compositions.

The five alkaline scoria samples all contain olivine, augite, and hornblende. The most silicic, S20, also contains bronzite and plagioclase. The others contain occasional rounded plagioclase crystals and rare bronzite usually rimmed by augite. S31 and S33, from the most incompatible-element-rich horizon, also contain phlogopite. The general absence of plagioclase and bronzite in the alkaline

scoriae, and the presence of phlogopite in the most enriched samples strongly support a connection with the basanite-minette series magmas, for which these are typical characteristics. Plagioclase and bronzite are widespread in V. Colima's products, and phlogopite is otherwise unknown.

The alkaline ash A38 is dominated by chromite-rich olivines and large twinned augites, and contains <2 vol% microphenocrystic plagioclase. This mineralogy, and its high concentrations of P_2O_5 and other incompatible elements give A38 the unmistakable signature of a basanite. Unlike the other studied horizons, this ash sequence probably did not erupt from V. Colima. Its likely source is a basanite cinder cone to the NW, although the measured thickness of 3 m seems inconsistent with a vent distance of 20–35 km; as suggested by one of the reviewers, perhaps it issued from a closer, as yet undiscovered vent.

Mineral Compositions

Mineral compositions were investigated by electron microprobe in 8 scoria samples: 4 calc-alkaline – S3, S16, S22, S36, and 4 alkaline – S20, S33, S34, S35. All minerals were analyzed on an 8-channel ARL microprobe at 15 kv accelerating potential. Minerals of similar composition to the unknowns were used as standards. Sample currents were 10 nA for plagioclase and 30 nA for other minerals.

Plagioclase. In the calc-alkaline basalt (LC-II), plagioclase microphenocrysts and groundmass crystals range in composition from An_{80} to An_{60}. V. Colima's post-caldera lavas (LC-I) contain a wide range of plagioclase compositions (An_{16-85}) with most between An_{40} and An_{60}. Andesine-labradorite crystals in these calc-alkaline samples typically have very low K_2O contents (0.05–0.2 wt.%). Groundmass andesine-labradorite crystals in the basanite-minette samples have much higher K_2O contents (0.5–1.7 wt.%). In the four analyzed calc-alkaline scoria samples, plagioclase shows the same wide compositional range and low K_2O contents as for post-caldera lavas. No correlation of plagioclase composition versus whole rock SiO_2 content is apparent.

Among the four alkaline scoriae, the abundance of plagioclase varies inversely with the concentration of incompatible elements. The most enriched samples (S31, S33, S34) contain <2 vol% plagioclase, which often occurs as rounded, resorbed crystals. Plagioclase rim compositions in these four samples range from An_{40-52} and contain 0.2–0.5 wt.% K_2O, a reflection of relatively high whole-rock K_2O contents. Core compositions can be either more or less An-rich, but generally show the low-K_2O, calc-alkaline signature.

Augite, Bronzite, and Olivine. Figure 7 shows augite, bronzite, and olivine analyses for the eight scoria samples plotted in the left half of the Ca-Mg-Fe pyroxene quadrilateral. Rim and core analyses are indicated by open and closed circles respectively. For comparison, the upper left diagram shows data for the calc-alkaline basalt (star), post-caldera lavas (triangles), and basanite-minette samples (circles) taken from LC-I and LC-II. The calc-alkaline and basic alkaline suites are easily distinguished by the higher Wo content in augite, higher Fo content in olivine, and lack of bronzite in the basanites and minettes.

Calc-alkaline scoria S3 contains normally zoned augite and bronzite. Rim analyses are given in Table 4. Bronzite phenocryst cores range to En_{84}, much more Mg-rich than bronzite from post-caldera lavas (En_{70-76}). Calc-alkaline scoria S16 contains reversely zoned augite and complexly zoned bronzite ranging from En_{70-82}. Olivine shows simple normal zoning from Fo_{87} cores to Fo_{82} rims. Calc-alkaline scoria S-22 has a very simple mafic mineralogy; bronzite is normally zoned from En_{77} cores to En_{70} rims, augite is unzoned, and olivine is absent. Pyroxene rim compositions are given in Table 4. The remaining calc-alkaline scoria sample (S36) contains relatively unzoned bronzite (En_{70}) with one more Mg-rich core (En_{75}). Augite rims are homogeneous, but cores are both higher and lower in Mg and Ca. Pyroxene rim compositions from S36 are given in Table 4. Olivine shows normal zoning from Fo_{86} cores to Fo_{81} rims.

All four of the alkaline scoria samples contain augite crystals similar to those in S36: both normally and reversely zoned crystals with homogeneous rims. The Mg–Ca-rich, normally zoned augite cores are similar to augite cores in basanites and minettes, while the Fe-rich, reversely zoned

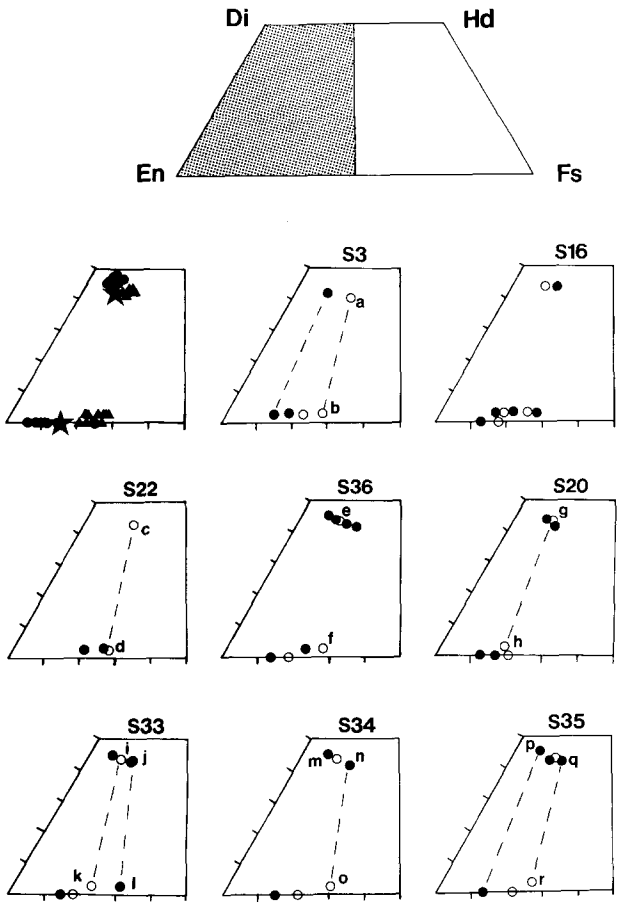

Fig. 7. Average microprobe analyses of augite, bronzite, and olivine subpopulations plotted in the left half of a mol% pyroxene quadrilateral. The upper left diagram shows analyses from post-caldera lavas (*triangles*) and the calc-alkaline basalt (star), and basanite-minette samples (*circles*) taken from LC-I and -II. Only augite core compositions have been plotted for basanite-minette samples. In plots for the 8 scoria samples, *open circles* are rim analyses and *closed circles* show core analyses. Probable equilibrium pyroxene pairs are connected by dashed lines. *Small letters a–r* correspond to analyses in Table 4

Table 4. Point microprobe analyses of pyroxenes

	S3	S3	S22	S22	S36	S36	S20	S20
	a	b	c	d	e	f	g	h
SiO_2	52.67	53.97	52.53	54.25	50.54	53.16	51.81	54.92
TiO_2	0.58	0.31	0.37	0.20	0.65	0.25	0.67	0.28
Al_2O_3	1.57	1.63	1.90	0.98	3.97	1.46	3.57	2.20
Cr_2O_3	0.03	0.08	0.01	0.02	0.15	0.06	0.14	0.06
FeO	10.46	17.60	8.90	17.73	7.30	17.52	7.00	12.26
MnO	0.25	0.34	0.27	0.42	0.14	0.37	0.16	0.27
MgO	15.41	25.39	15.37	25.81	15.58	25.52	15.88	29.40
NiO	0.01	0.03	0.00	0.01	0.01	0.01	0.03	0.05
CaO	19.85	1.63	20.91	1.35	21.22	1.33	21.34	1.35
Na_2O	0.52	0.06	0.40	0.05	0.40	0.04	0.46	0.04
Total	101.34	101.04	100.66	100.82	99.96	99.72	101.06	100.83
X_{Fe}	0.165	0.271	0.141	0.271	0.117	0.271	0.112	0.185
X_{Mg}	0.433	0.697	0.434	0.703	0.446	0.703	0.452	0.789
X_{Ca}	0.401	0.032	0.425	0.026	0.437	0.026	0.436	0.026

	S33	S33	S33	S33	S34	S34	S34	S35	S35	S35
	i	j	k	l	m	n	o	p	q	r
SiO_2	51.66	53.50	53.50	52.66	52.27	49.97	52.65	52.20	50.10	53.62
TiO_2	0.54	0.13	0.23	0.17	0.34	0.49	0.24	0.37	0.47	0.28
Al_2O_3	2.99	1.31	2.35	0.90	2.42	3.03	1.55	2.66	3.15	1.78
Cr_2O_3	0.04	0.00	0.01	0.00	0.38	0.21	0.03	0.70	0.01	9.03
FeO	6.33	8.62	14.42	19.57	5.02	9.14	19.32	4.61	9.12	16.87
MnO	0.16	0.50	0.31	0.49	0.10	0.18	0.40	0.10	0.24	0.33
MgO	16.35	15.00	28.04	24.68	16.87	15.17	24.89	16.79	15.13	26.25
NiO	0.01	0.00	0.00	0.00	0.02	0.00	0.00	0.01	0.04	0.03
CaO	21.55	21.41	1.25	1.09	22.23	20.25	1.16	21.88	20.35	1.45
Na_2O	0.48	0.57	0.06	0.04	0.36	0.47	0.03	0.45	0.50	0.03
Total	100.11	101.04	100.17	99.60	100.01	98.91	100.27	99.77	99.11	100.67
X_{Fe}	0.100	0.137	0.218	0.301	0.079	0.147	0.297	0.074	0.147	0.257
X_{Mg}	0.462	0.426	0.757	0.677	0.473	0.435	0.681	0.478	0.434	0.714
X_{Ca}	0.438	0.437	0.024	0.021	0.448	0.418	0.022	0.448	0.420	0.028

Small letters a–r correspond to points on Fig. 7

cores are similar to other calc-alkaline augites from V. Colima. In the youngest of the alkaline scoria (S20), bronzite is homogeneous at En_{80}. Most olivine crystals are Fo_{80}, but cores range to Fo_{87}. Pyroxene rim analyses are given in Table 4. In the highly alkaline, phlogopite-bearing scoria S33, rims of bronzite on augite cores, and rims of augite on bronzite cores are both observed. Bronzite crystals are all reversely zoned from En_{68} cores to En_{76} rims. Olivine crystals are normally zoned from Fo_{85} cores to Fo_{82} rims. Table 4 lists analyses of pyroxene rims and the reversely zoned cores. In the underlying alkaline scoria S34, a single bronzite crystal (En_{68}) was observed, rimmed by augite. Olivine is normally zoned from Fo_{85} cores to Fo_{79} rims. Table 4 gives analyses for the bronzite and augite cores. The oldest alkaline scoria sample (S35) also showed a single, augite-rimmed bronzite crystal (En_{71}). Olivines are normally zoned from Fo_{87} cores to Fo_{79} rims. Table 4 lists analyses of bronzite and augite cores.

Hornblende. Selected analyses of hornblende from the scoria samples are given in Table 5. None differ significantly from analyzed hornblendes in V. Colima's post-caldera andesites (LC-I). Of the calc-alkaline samples, S3 is nearly hornblende-free, S16 and S22 contain homogeneous hornblende, and that in S36 shows slight reverse zoning. Hornblendes are consistently reversely zoned in three of the alkaline scoriae (S20, S34, S35), and normally zoned only in the phlogopite-bearing S33. Hornblendes in the alkaline scoriae contain slightly higher K_2O and F than those from calc-alkaline samples but are otherwise indistinguishable. This is consistent with their probable origin in the calc-alkaline end-member prior to mixing.

Phlogopite. The phlogopite crystals of alkaline scoria S33 show slight normal zoning. Rim and core analyses are given in Table 5. They are somewhat more Fe-rich and Mg-poor than minette phlogopites (LC-II), but have similar TiO_2 (<3.4 wt.%) and F (<1 wt.%) contents.

Spinels. The most compositionally complex minerals in the Colima scoria samples are the spinels, which range from titanomagnetites as inclusions and groundmass crystals in the andesites, to various Cr–Al–Mg–Fe spinels as groundmass crystals, but particularly as inclusions in mafic

Table 5. Average microprobe analyses of hornblende and phlogopite

	Hornblende								Phlogopite	
	S16	S22	S33r	S33c	S34r	S34c	S35r	S35c	S33r	S33c
SiO_2	43.10	43.19	42.92	42.21	42.18	41.91	41.18	42.25	37.43	37.55
TiO_2	2.65	2.49	1.64	2.23	2.33	2.21	3.00	2.05	3.36	2.72
Al_2O_3	12.16	12.19	12.55	13.19	13.03	13.16	13.85	12.44	16.74	16.07
Cr_2O_3	0.06	0.04	0.07	0.03	0.04	0.01	0.07	0.00	0.19	0.42
FeO	11.87	12.24	11.63	10.57	9.43	11.64	10.30	12.40	7.95	6.87
MnO	0.10	0.12	0.12	0.12	0.09	0.10	0.10	0.17	0.04	0.05
NiO	0.01	0.00	0.00	0.02	0.01	0.01	0.01	0.00	0.06	0.00
MgO	14.78	14.60	15.24	15.54	16.14	14.94	15.11	14.53	20.08	21.34
BaO	0.01	0.01	0.01	0.00	0.01	0.01	0.02	0.00	0.83	0.53
CaO	11.40	11.33	11.06	11.57	11.86	11.44	11.47	10.91	0.06	0.07
SrO	0.08	0.10	0.15	0.25	0.16	0.13	0.12	0.08	0.15	0.10
Na_2O	2.70	2.64	2.60	2.65	2.49	2.57	2.85	2.63	0.86	0.83
K_2O	0.32	0.28	0.62	0.92	1.08	0.89	0.47	0.34	8.74	7.79
F	0.11	0.11	0.15	0.32	0.38	0.29	0.18	0.17	0.75	0.90
Cl	0.03	0.03	0.02	0.02	0.02	0.02	0.01	0.01	0.01	0.01
H_2O*	2.01	2.01	1.98	1.92	1.88	1.91	1.97	1.95	3.82	3.71
$-O=F+Cl$	0.06	0.06	0.07	0.14	0.17	0.13	0.08	0.08	0.32	0.38
Total	101.33	101.32	100.69	101.42	100.96	101.11	100.63	99.85	100.75	98.58

r-rim, c-core analyses; H_2O* calculated from stochiometry

Table 6. Average microprobe analyses of spinel subpopulations

	S3	S16	S16	S22	S36	S20	S20	S33	S34	S34	S35	S35
	a	b	c	d	e	f	g	h	i	j	k	l
SiO_2	0.08	0.11	0.02	0.08	0.11	0.12	0.10	0.12	0.07	0.06	0.04	0.19
TiO_2	14.27	0.34	1.44	8.43	11.46	8.25	0.49	5.65	1.07	5.89	1.57	9.93
Al_2O_3	2.00	14.99	26.27	3.20	3.93	4.28	7.54	4.91	12.89	2.98	7.80	3.92
V_2O_5	0.98	0.05	0.32	0.54	0.83	0.43	0.07	0.23	0.09	0.40	0.17	0.66
Cr_2O_3	0.22	45.52	23.77	0.09	0.35	0.64	34.66	0.33	43.48	0.08	42.22	0.39
FeO	75.67	29.03	35.67	80.15	75.16	76.71	46.41	76.84	30.17	83.67	39.03	74.24
MnO	0.32	0.30	0.19	0.23	0.29	0.20	0.33	0.29	0.26	0.25	0.37	0.30
MgO	2.58	9.14	11.36	2.81	4.61	4.80	7.07	6.49	11.16	2.29	6.82	4.58
NiO	0.02	0.08	0.26	0.00	0.00	0.16	0.12	0.00	0.15	0.00	0.12	0.00
Total	96.14	99.56	99.30	95.53	96.74	95.59	96.79	94.86	99.34	95.62	98.14	94.21
Recalculated analyses												
Fe_2O_3*	39.10	9.43	17.65	49.99	44.05	49.62	27.12	55.21	13.85	55.52	17.20	45.29
FeO	40.49	20.55	19.79	35.16	35.52	32.06	22.00	27.15	17.70	33.71	23.55	33.48
Total	100.06	100.51	101.07	100.53	101.15	100.56	99.50	100.38	100.72	101.18	99.86	98.74

* Ferric iron recalculated following Carmichael (1967)

phenocrysts of more basic samples. Analyses of selected spinels are given in Table 6.

The relatively silicic calc-alkaline andesite scoriae S3 and S22 contain only titanomagnetites similar to those in post-caldera lavas (Table 6a and d). Groundmass spinel was not observed in the relatively basic calc-alkaline scoria S16. Four Cr – Al – Mg – Fe spinels included in olivine and bronzite crystals show broad compositional variability; one (c) is similar to spinel of the calc-alkaline basalt, while other chromites (b) are richer in Fe and Al and poorer in Mg than those in basanites and minettes. The fourth calc-alkaline sample (S36) contains homogeneous groundmass titanomagnetite (e), other titanomagnetite inclusions in unzoned bronzite and reversely zoned augite, and chromite inclusions in normally zoned olivine.

As is true for augite, the alkaline scoria samples generally contain spinels similar to those in S36: groundmass titanomagnetite (f, h, j, l), with other titanomagnetites as inclusions in pyroxenes and hornblendes (usually reversely zoned), and chromites as inclusions in normally zoned olivines (g, i, k). Analyzable chromites were not encountered in the phlogopite-bearing S33.

The chromites present in both alkaline and calc-alkaline scoria samples are similar to chromites in the basanite-minette suite. With the exception of spinel (c) in S16, they are unlike spinels in the calc-alkaline basalt. The ground-

mass and included titanomagnetites in these scoria samples are broadly similar to those in post-caldera andesitic lavas. Thus, three alkaline scoriae and even two calc-alkaline scoriae contain olivines and included chromites which may have originated in basanite-minette magmas. The titanomagnetites of the alkaline scoria samples probably originated in the calc-alkaline magmas of V. Colima.

Discussion: The Alkaline Scoriae

A variety of geological, mineralogical, and compositional evidence supports the interpretation that the alkaline scoria horizons represent pre-eruptive mixtures of basanite-minette magma and calc-alkaline magma. The alkaline scoriae erupted from Colima's pre-caldera cone over a period of at least 2,000 years, beginning before 8,300 years ago (Fig. 5). Morphologically estimated ages for the basanite-minette cones of 1,500–>20,000 years (LC-II), and the presence of the crystal-enriched basanitic ash A38 immediately below the alkaline scoriae, demonstrate that basanite-minette magma was erupting just 20 km away from V. Colima during the period that it produced the anomalously alkaline scoriae. Alkaline scoria layers S34 and S31–S33 are among the thickest and coarsest-grained horizons in the studied sections, probably reflecting unusually powerful eruptions. Just beneath them, occurs scoria S36, the most basic calc-alkaline sample yet encountered on Colima's upper cone.

The alkaline scoriae contain hornblende and small amounts of bronzite and plagioclase, phases which characterize V. Colima's andesites. They also contain cores of Mg–Ca-rich augite, chromites, phlogopites, and high-K_2O plagioclase rims similar to phases in the basanite-minette magmas. The alkaline scoriae show the high incompatible-element contents typical of basanite-minette magmas and plot between the two major Colima suites on compositional variation diagrams.

Finally, compositional zoning patterns of mafic phenocrysts in the alkaline scoriae also support a mixing origin. Chromite-bearing olivines are all normally zoned, while bronzite and hornblende crystals are usually reversely zoned. Augite rims are compositionally homogeneous, but cores can be either Mg–Ca-rich, like basanite-minette augite cores, or relatively Fe-rich, similar to augites of Colima's andesites. The low-temperature end-member magma was probably a typical two-pyroxene, hornblende-andesite. The high-temperature end-member was probably a minette containing olivine, chromite, augite, and phlogopite. The most extreme product of this mixing (S33) contains the unusual assemblage olivine, augite, bronzite, hornblende, phlogopite, plagioclase, and titanomagnetite in apparent textural equilibrium.

In an attempt to model the proposed mixing event geochemically, we performed a number of major-element least-squares calculations (Wright and Doherty 1970) to derive the alkaline scoria samples S33 and S34 by combining a minette (LC-II) with a Colima andesite (LC-I) and allowing olivine separation. The best results (lowest Σr^2) were obtained by combining minette 7E with andesite Col-15 and removing 3–4% olivine (Table 7). The end-member proportions predicted from the major-element fit were then used to predict trace-element concentrations for S33 and S34. The predicted compositions match the analyzed values (Table 3 reasonably well. The discrepancy in Cr can be eliminated by just 0.04% separation of chromite (45% Cr_2O_3). Predicted concentrations of Rb, Sr, Y, Zr, Ba, and Hf are all too high, but the chosen alkalic end-member (7E) is the richest of the basanite-minette samples in each of these elements. Inspection of Fig. 4 shows that the choice of another basanite-minette sample in the mixing calculations can eliminate the discrepancies in these elements as well. The calculations call for 46 wt.% minette component in S34, and 61% in the phlogopite-bearing S33.

The pre-mixing temperature of the andesitic end-member can be estimated from pyroxene geothermometry (Wells 1977) using core compositions of reversely zoned crystals in S33 (Fig. 7 and Table 4). The calculated temperature, 940° C, is similar to pre-eruptive temperatures estimated in LC-I for Colima's andesitic lavas. The post-mixing, pre-eruptive temperature of S33, estimated from pyroxene rim compositions (Fig. 7 and Table 4) is about 1,040° C. The mass proportions derived from the mixing

Table 7. Magma Mixing Models for the Origin of S33 and S34

	7E	Col-15	Oliv	Pred. S33	S33	Pred. S34	S34
Major elements normalized anhydrous (wt.%)							
SiO_2	49.72	58.19	40.81	53.53	53.55	55.02	54.84
TiO_2	1.69	0.79	–	1.37	1.05	1.24	0.98
Al_2O_3	11.99	17.61	–	14.70	14.94	15.75	16.12
FeOt	7.29	6.19	11.06	6.72	7.09	6.49	6.97
MnO	0.11	0.12	0.21	0.11	0.12	0.11	0.13
MgO	12.18	4.19	47.67	7.77	7.82	6.04	6.04
CaO	8.58	7.09	0.25	8.21	8.50	8.07	8.14
Na_2O	3.38	4.45	–	3.93	3.41	4.14	3.85
K2O	3.69	1.18	–	2.75	2.88	2.39	2.44
P_2O_5	1.36	0.19	–	0.91	0.64	0.74	0.49
Trace elements (ppm)							
Sc	27	19	–	24	24	23	25
V	265	179	–	237	190	226	193
Cr	691	75	–	453*	330	361*	189
Ni	436	51	1,400	245*	93	174*	40
Cu	90	23	–	65*	90	54	62
Zn	80	66	–	77	71	75	72
Rb	73	16	–	51*	24	43*	26
Sr	3,079	584	–	2,123*	2,689	1,755*	1,434
Y	29	20	–	26*	21	25*	22
Zr	554	131	–	393*	232	331*	198
Cs	1.0	0.4	–	0.8	0.6	0.7	0.4
Ba	4,230	413	–	2,754*	1,767	2,185*	792
La	82	10	–	54	54	44	34
Ce	188	25	–	125	121	101	82
Nd	93	15	–	63	67	51	49
Sm	15.2	3.0	–	10.5	9.6	8.7	8.3
Eu	4.5	1.0	–	3.2	2.5	2.7	2.3
Tb	1.2	0.45	–	0.92*	0.69	0.81*	0.68
Dy	5.5	2.9	–	4.6*	3.7	4.2	4.0
Yb	1.7	1.8	–	1.7	1.5	1.8	1.7
Lu	0.18	0.25	–	0.21	0.19	0.23	0.20
Hf	17.9	3.1	–	12.2*	6.3	10.0*	5.1
Th	7.13	1.5	–	5.0	4.7	4.1	4.1
U	2.41	0.6	–	1.7	1.5	1.4	1.3

Mixing equations:
$S33 = 0.61(7E) + 0.42(Col\text{-}15) - 0.03(Oliv)$: $\Sigma r^2 = 0.74$
$S34 = 0.46(7E) + 0.58(Col\text{-}15) - 0.04(Oliv)$: $\Sigma r^2 = 0.62$

* Indicates unsatisfactory fit

calculations allow an estimate of the minette temperature as about 1,110° C, consistent with temperature estimates for basanite-minette samples based on oxygen isotope partitioning (LC-II).

Summary and Conclusions

Where exposed in roadcuts 6 km downwind from Colima's active crater, ash- and scoria-fall deposits have been accumulating at a rate of 1.3 m/1,000 years since the close of the Pleistocene. Empirical modelling of eruptive volumes based on published studies of Mt. St. Helens 1980 fall-units allows an estimate of magma eruptive rate for fall-material of 0.31 km^3/1,000 years, which is less than 15% of the estimated lava eruption rate at Colima. A thick, normally-graded, and coarse-grained scoria-fall horizon bounded by carbon dates of 3,400 and 4,740 years is thought to have been deposited during Colima's caldera-forming eruption, independently dated at 4,300 yrs.

The majority of scoria and ash samples from the studied sections are calc-alkaline hornblende-andesites which cluster tightly in composition between 57 and 59% SiO_2, similar to scoriae from Colima's 1913 Pelean-type eruption and from the caldera-forming eruption. This composition must be accepted as the dominant pyroclastic eruptive product of V. Colima at present, just as 60–61% SiO_2 andesites dominate as lavas.

An unusual sequence of ash- and scoria-fall deposits occurs just beneath the oldest ^{14}C age of 8,300 years. The sequence begins with 3 m of crystal-enriched basanite ash, presumably derived from a nearby cinder cone. The basanite ashes are overlain by coarse-scoria and ash horizons showing progressive upward increases in a large number of incompatible elements and culminating in a phlogopite-bearing scoria layer. These alkaline scoriae are viewed as the products of mixing between calc-alkaline andesites from V. Colima and basanite-minette magmas that were erupting from cinder cones just 20 km away during the late-Quaternary. Chemical mixing models indicate 60% minette component in the phlogopite-bearing alkaline scoriae.

Acknowledgements. We wish to thank the following people who helped in the tedious and uncomfortable work of describing and sampling the sections and searching for charcoal: Debbie Cave, Connie Frisch, Anthony Lomax, and Karen Prestegaard. The US Customs office at Nogales AZ carefully dried many of the charcoal samples, and James Buckley at Teledyne Isotopes produced the radiocarbon ages. Helen Michel and Frank Asaro performed the INA analyses and Joachim Hampel analyzed whole-rock alkalies. Thoughtful reviews by Wes Hildreth and Michael Sheridan greatly improved the logic and language of the paper. This work was supported by NSF EAR 80-06043 (Carmichael) and Penrose Grant 2487-79 (Luhr).

Appendix 1. Description of sampled scoria and ash horizons

Sample	Section	D (cm)	T (cm)	A (cm)	Comment
S1	A	0	10	6	surface scoria layer; underlain by 10 cm soil-ash
S2	A	20	10	5	underlain by 30 cm soil-ash
S3	A	60	10	4	
A4	A	70	100	0.5	ash with purple-brown base, blue-grey top
S5	A	170	15	6	underlain by 15 cm ash
S6	A	200	45	5	underlain by 10 cm soil-ash
S7	A	255	10	4	underlain by 20 cm soil-ash
S8	A	285	140	10	coarser toward base; underlain by 40 cm ash equivalent to A9
A9	B	425	40	0.5	lower 25 cm is blue-grey ash, upper 15 cm is brown ash-soil
S10	B	465	15	6	underlain by 10 cm soil-ash
S11	B	490	10	3	underlain by 15 cm soil-ash
S12	B	515	15	4	underlain by 7 cm soil-ash
S13	B	535	15	4	equivalent to S15
S14	B	550	25	7	upper 10 cm is dark ash and scoriae; equivalent to S16
S15	C	540	33	4	equivalent to S13
S16	C	570	25	4	equivalent to S14 with upper dark 10 cm
A17	C	595	50	0.5	charcoal abundant in upper levels
S18	C	645	25	4	
A19	C	670	60	0.5	no charcoal
S20	C	730	33	6	
A21	C	765	15	0.5	ash-soil
S22	C	780	33	8	lower 5 cm fine blue lithics underlain by 4 cm soil-ash
S23	C	815	10	3	
A24	C	865	25	0.5	prominent blue (25 cm) ash overlain by 30 cm pink ash and finally by 10 cm blue ash; sample from lower bed
S25	C	890	65	5	coarsens toward top; very lithic rich; equivalent to S32
A26	C	955	10	0.5	
S27	C	965	22	3	underlain by 4 cm soil-ash
S28	B	990	20	4	underlain by 5 cm soil-ash
S29	B	1,015	15	6	grey-brown scoriae with small white inclusions; underlain by 4 cm soil-ash
S30	B	1,035	6	4	underlain by 250 cm reworked ash and scoriae with abundant charcoal
S31	B	1,290	>20	4	at base of section B; altered buff scoriae with abundant phlogopite; equivalent to S33
S32	D	890	45	6	equivalent to S25; underlain by 135 cm sequence of reworked ash and scoriae with abundant charcoal

Appendix 1 (continued)

Sample	Section	D (cm)	T (cm)	A (cm)	Comment
S33	D	1,070	70	10	coarse buff colored scoriae with abundant phlogopite; equivalent to S31; underlain by 20 cm ash
S34	D	1,160	190	14	coarse blue-grey scoriae; underlain by 10 cm ash
S35	D	1,360	30	4	underlain by 4 cm ash
S36	D	1,395	75	7	very fresh, dark scoriae underlain by 5 cm ash
S37	D	1,475	200	9	underlain by 40 cm ash and scoriae, 45 cm of bedded grey pumice with a lithic rich top, followed by 30 cm of interbedded pumice and red ash
A38	D	1,790	300	0.5	thin bedded ash, sampled from the top; base is pink and fine-grained
S39	D	2,090	50	6	underlain by 10 cm pink ash
S40	D	2,150	75	5	very fresh dark scoriae underlain by 150 cm of interbedded, 10–20 cm thick ash and scoriae
S41	D	2,375	80	5	underlain by some 300 cm of 10–30 cm thick layers of ash and scoriae; two prominent scoria horizons were sampled as S42 and S43
S42	D	2,545	30	7	begins 90 cm below S41
S43	D	2,610	20	5	begins 35 cm below S42
S44	D	2,675	70	6	underlain by 700 cm of interbedded ash (10–15 cm) and scoria layers (10–60 cm) overlying a base of volcanic breccia; many scoriae badly altered; two prominent scoria horizons were sampled as S45 and S46
S45	D	3,190	20	7	begins 445 cm below S44
S46	D	3,305	100	5	begins 560 cm below S44

D = depth to top of layer from top of S1; T = thickness of layer; A = average of three largest scoriae
Preface S- indicates scoria sample and A- indicates ash sample

Appendices 2 (whole rock XRF analyses) and 3 (Modes) are available upon request

References

Aramaki S (1979) Iwanami-shoten. Earth Sci 7:72, Tokyo

Baker PE, Holland JG (1973) Geochemical variations in a pyroclastic succession on St. Kitts, West Indies. Bull Volcanol 37:472–490

Carmichael ISE (1967) The iron-titanium oxides of salic volcanic rocks and their associated ferromagnesian silicates. Contrib Mineral Petrol 14:36–64

Demant A (1979) Vulcanologia y petrographia del sector occidental del eje neovolcanico. Univ Nal Autón México. Inst Geol Revista 3 (1):39–57

Luhr JF (1981) Colima: History and cyclicity of eruptions. Volcano News 7:1–3

Luhr JF, Carmichael ISE (1980) The Colima volcanic complex: I. Postcaldera andesites from Volcán Colima. Contrib Mineral Petrol 71:343–372

Luhr JF, Carmichael ISE (1981) The Colima volcanic complex: II. Late-Quaternary cinder cones. Contrib Mineral Petrol 76:127–147

Perlman I, Asaro F (1969) Pottery analysis by neutron activation. Archaeometry 11:21–52

Sarna-Wojcicki AM, Shipley S, Waitt RB Jr, Dzurisin D, Wood SH (1981) The 1980 eruptions of Mt St Helens, Washington: Areal distribution, thickness, mass, volume, and grain size of air-fall ash from the six major eruptions of 1980. USGS Prof Pap 1250:577–600

Ui T (1981) Dry avalanche – Mechanism of eruption, transportation and deposition. IAVCEI Symposium on arc volcanism, abstr pp 388–389, Tokyo

Voight B, Glicken H, Janda RJ, Douglass PM (1981) The 1980 eruptions of Mt St Helens, Washington: Catastrophic rockslide avalanche of May 18. USGS Prof Pap 1250:347–377

Waitt RB Jr, Dzurisin D (1981) The 1980 eruptions of Mt St Helens, Washington: Proximal air-fall deposits from the May 18 eruption – stratigraphy and field sedimentology. USGS Prof Pap 1250:601–616

Waitt RB Jr, Hansen VL, Sarna-Wojcicki AM, Wood SH (1981) The 1980 eruptions of Mt St Helens, Washington: Proximal air-fall deposits of eruptions between May 24 and August 7, 1980 – stratigraphy and field sedimentology. USGS Prof Pap 1250:617–628

Waitz P (1906) Le volcan de Colima. 10^{e} Congr Geol Intern, Mexico, Guide excursion XIII:28

Wells PRA (1977) Pyroxene thermometry in simple and complex systems. Contrib Mineral Petrol 62:129–139

Wilcox RE (1954) Petrology of Paricutin Volcano, Mexico. US Geol Surv Bull 965-C:281–349

Wright TL, Doherty PC (1970) A linear programming and least squares computer method for solving petrologic mixing problems. Geol Soc Am Bull 81:1995–2008

Received January 25, 1982; Accepted June 19, 1982